Evaluation of Radiological Dose Variability at Exclusion Area Boundary Considering Short-term Transient Wind Scenarios

Jemo Ryu[a], Jaehyun Cho[a]
[a] Chung-Ang University, 84, Heukseok-ro, Dongjak-gu, Seoul, Republic of Korea
jemo2000@cau.ac.kr

Abstract: Consequence evaluation at the Exclusion Area Boundary is frequently performed under an assumed fixed wind direction, whereas actual emergency conditions may involve rapid changes in wind direction over short time windows. This study develops a computational fluid dynamics-based framework to evaluate radiological dose variability at the EAB under short-term transient wind scenarios, with emphasis on how time-varying wind direction alters near-field atmospheric dispersion. Transient wind conditions are prescribed to represent short-duration wind shifts, and unsteady simulations are conducted over a plant-site computational domain to obtain time-dependent radionuclide concentration fields. The concentration fields are then converted to external effective dose-rate and cumulative dose metrics using dose conversion factors, and the resulting dose measures are extracted at multiple receptor locations along the EAB. By organizing dose responses in terms of temporal peaks, sector-wise variations, and receptor-to-receptor spread, the proposed workflow is intended to support EAB consequence evaluation and protective-action planning under rapidly evolving wind conditions.

1. INTRODUCTION

Protective-action decision making during a radiological release requires realistic, time-dependent estimates of airborne radionuclide concentrations near the Exclusion Area Boundary (EAB). Computational Fluid Dynamics (CFD) is particularly attractive for this purpose because it resolves building geometry, captures wake-induced recirculation, and reproduces channeling and vortex shedding that conventional Gaussian-type formulations cannot represent. Previous CFD applications at nuclear power plants [1, 2] have demonstrated that resolving site-scale flow features can substantially modify predicted plume pathways and short-range concentration footprints relative to integral models. Separately, correlation-based near-field treatments such as the Ramsdell–Fosmire (RAF) model [3] have shown that the choice of dispersion parameterization alone can alter estimated EPZ radii by up to roughly fifty percent; however, such parameterizations assume a temporally stationary wind direction and cannot capture the spatially resolved transient flow features that a CFD approach provides.

A practical limitation common to most published CFD-based assessments is the assumption that the inflow wind remains aligned with a single direction throughout the release. Meteorological observations at coastal sites show that the prevailing wind vector can rotate appreciably over time intervals comparable to the duration of a short atmospheric release [4], causing the plume centerline to migrate between EAB sectors and making the exposure at any receptor a strong function of when and how rapidly the shift takes place.

The present work develops a CFD-based framework that explicitly accommodates short-term transients in wind direction and evaluates the resulting time-dependent concentration fields at EAB receptors. An envelope computational domain is constructed to support any incoming wind direction without re-meshing; the velocity field is advanced across each wind-direction switch using unsteady Large Eddy Simulation (LES) with a transition treatment that dissipates residual momentum from the prior wind state; and the concentration fields produced by Lagrangian particle tracking are extracted at sixteen EAB azimuthal receptors. The framework is demonstrated for the Saeul Nuclear Power Plant Units 1 and 2 site (APR1400).

2. SITE GEOMETRY AND COMPUTATIONAL DOMAIN

Geometric modeling of the plant site and the surrounding computational domain establishes the basis for every subsequent step in the workflow. Two requirements drove the modeling choices reported in this section. The first was that structures expected to influence near-field flow needed to be represented with sufficient detail to capture wake and channeling effects within the EAB. The second was that the outer domain had to be large enough to admit arbitrary wind directions without inflow contamination or outflow reflection in the region where dose is evaluated.

2.1. Plant-Site Representation

The Saeul Units 1 and 2 site (APR1400) was selected as the reference plant for demonstration. The site model retains the principal buildings that govern local atmospheric flow: the reactor building complex, including the containment structures and the directly attached auxiliary buildings of both units, together with the turbine buildings located adjacent to the reactor groups. These primary structures were modeled because they generate the dominant near-field wake systems, recirculation cavities, and rooftop separation zones that shape plume behavior in the immediate vicinity of the release point.

In addition to the principal structures, a set of secondary buildings and outdoor facilities located inside the EAB was incorporated. This set includes representative support buildings, the condensate storage tanks and their associated yard structures, and several smaller plant facilities distributed across the site. Although individually small, these features collectively alter the streamwise pressure gradient, generate localized vortex shedding, and modify the path of low-elevation particle transport that would otherwise be predicted by a simplified two-building idealization. The resulting site geometry is shown in Fig. 1.

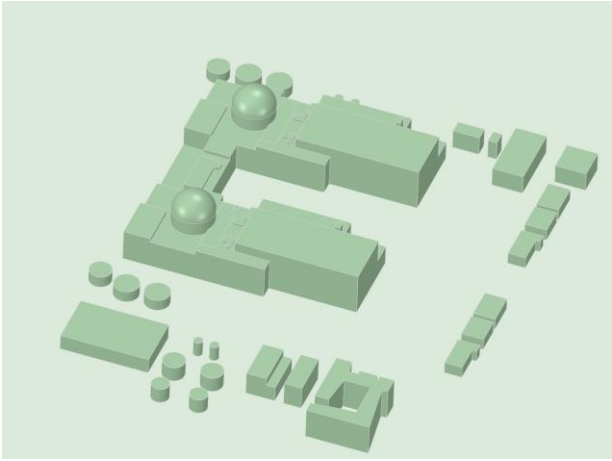

Fig. 1. Site geometry model for the Saeul Units 1 and 2 plant (APR1400)

2.2. Definition of the Computational Area

The EAB at the Saeul Units 1 and 2 site is defined as a circle of 560 m radius centered on the reactor vessel, in accordance with the site-specific licensing basis. The boundary is shown in Fig. 2 together with the locations of the principal plant structures. For the concentration evaluation reported in this work, the EAB perimeter was discretized into sixteen receptors corresponding to the conventional meteorological compass sectors (N, NNE, NE, ENE, E, ESE, SE, SSE, S, SSW, SW, WSW, W, WNW, NW, NNW). Each receptor is located at the intersection of its sector bearing with the EAB curve, taken from the nominal release point. This sixteen-sector arrangement was selected so that the angular resolution of the output matches the convention used in conventional consequence codes and so that the result remains directly comparable with site emergency planning documentation. To ensure that the analysis encompasses the full EAB with adequate margin, the computational extent for the near-field evaluation was set to 680 m from the center point.

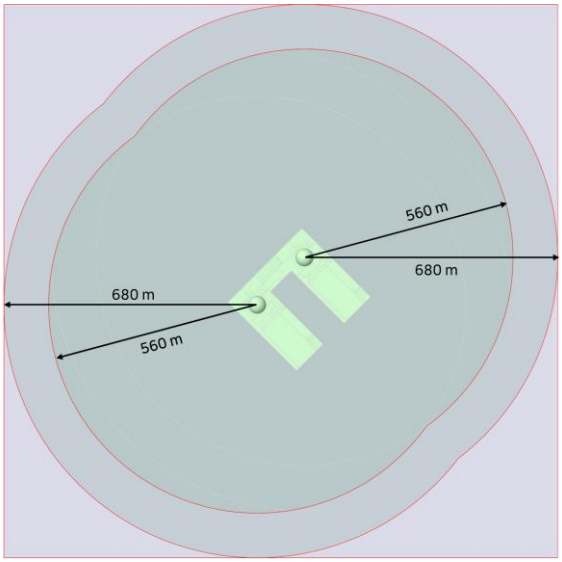

Fig. 2. Computational area of the Saeul Units 1 and 2 site and locations of the principal plant structures.

2.3. Envelope Computational Domain for Variable Wind Direction

When wind direction is permitted to change in time, a domain shaped for a single inflow vector is no longer adequate. A long, narrow rectangular box oriented along the prevailing wind is computationally efficient for a fixed-direction analysis, but rotating it during a simulation would require either remeshing or interpolation onto a new grid, both of which introduce inconsistencies in the velocity field. The strategy adopted here avoids these difficulties by constructing a single envelope domain that is large enough to encompass any direction-aligned sub-domain that may be required during the simulated sequence.

The envelope was generated by taking the rectangular sub-domain that would be used for any one of the sixteen sector directions and rotating it through the full 360° range. The geometric union of all these rotated rectangles forms a roughly circular envelope that extends beyond the 680 m analysis range in all horizontal directions. Vertically, the domain is capped at 1,000m, which is sufficient to contain the vertical extent of particle dispersion expected from the elevated release points considered. The resulting envelope domain is shown in Fig. 3.

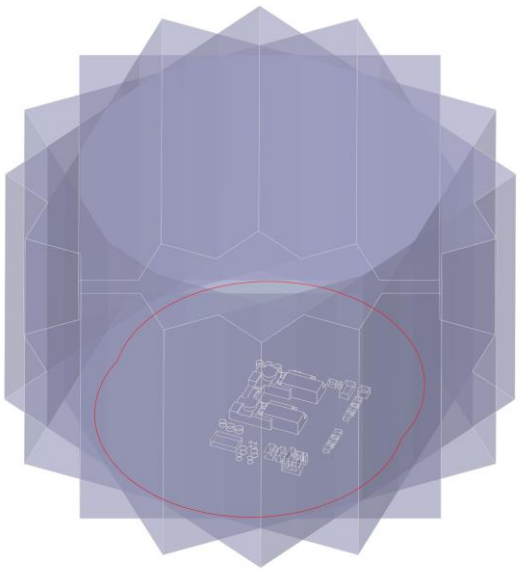

Fig. 3. Envelope computational domain sized to accommodate any wind direction, with the plant site located in the central region and direction-aligned sub-domains nested inside the envelope.

3. CFD METHODOLOGY FOR TIME-VARYING WIND DIRECTION

This section describes the numerical machinery used to advance the velocity field through a sequence of wind-direction changes without compromising temporal continuity. The treatment is built around two principles. First, the velocity field must evolve in time under a continuously updated boundary forcing rather than being replaced by separately precomputed steady-state solutions for each wind direction, because such replacement breaks the temporal causality on which subsequent particle-transport calculations depend. Second, the moment of a wind-direction switch must be handled with care so that the residual momentum present in the active domain does not corrupt the new flow state.

3.1. Governing Equations and Turbulence Closure

The carrier-phase flow is treated as unsteady, incompressible Newtonian air at neutral atmospheric stability. The filtered Navier–Stokes equations are solved using Large Eddy Simulation, which resolves the energy-containing eddies responsible for the wake structures of interest and models only the smallest scales. Subgrid-scale closure is provided by the Wall-Adapting Local Eddy-viscosity (WALE) model, selected because it returns the correct asymptotic wall behavior in the presence of complex geometries and does not require ad hoc damping functions near solid surfaces. All simulations were performed with ANSYS Fluent using a pressure-based segregated solver, bounded second-order schemes for the convective fluxes, and a second-order implicit advancement in time. The time step was chosen so that the convective Courant number based on the local mean velocity and the grid spacing remained below unity over the majority of the active domain.

Once a velocity field is available, radionuclide transport is computed using the Discrete Phase Model (DPM) in a Lagrangian framework. Particles are released continuously at the source location with prescribed mass flow rate, size distribution, and density, and their trajectories are integrated using the instantaneous carrier-phase velocity. Because the particle equations of motion depend on the local velocity at every time step, the carrier-phase field must remain temporally continuous; any instantaneous discontinuity introduced by, for instance, swapping in a separately computed steady-state field for a different wind direction would generate spurious particle acceleration events and unphysical trajectory excursions during the transition. The active-domain reconfiguration scheme described below was developed specifically to avoid such discontinuities.

3.2. Active-Domain Reconfiguration

The envelope domain introduced in Section 2.3 is too large to be used in its entirety for a single wind direction: doing so would waste cells in regions where the flow is essentially parallel to a lateral boundary and where boundary-condition treatments would distort the local solution. To exploit the envelope efficiently, only a direction-aligned rectangular sub-domain is kept active at any one time, while the remainder is deactivated. Activation is implemented through Fluent's cell-zone enable/disable mechanism, which preserves the mesh and the cell connectivity but excludes deactivated cells from the linear system solved at each iteration.

Fig. 4 (a) illustrates the configuration for a north-wind condition. The active rectangle is aligned with the north–south axis. The northern face of the rectangle is assigned as a velocity inlet and supplied with the prescribed wind-speed magnitude together with a logarithmic vertical profile representative of neutral atmospheric stability. The southern face is assigned as a pressure outlet. The two lateral faces are assigned as slip walls at the envelope boundary so that the simulation does not require explicit information about flow outside the active region. The remaining envelope cells are inactive and do not participate in the solution

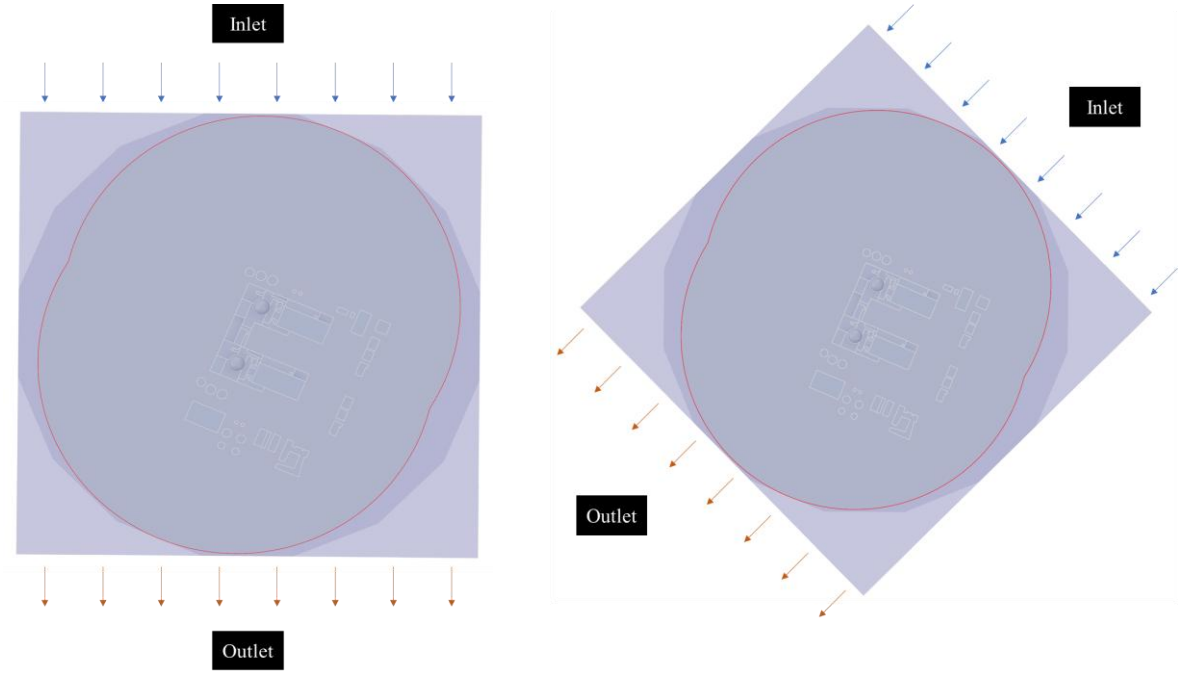

(a) North-wind direction, with the northern face as wind inlet and the southern face as wind outlet.

(b) Updated configuration after a northeast-wind direction, with the north-eastern face as wind inlet and the south-western face as wind outlet.

Fig. 4. Active rectangular sub-domain and boundary assignments for wind-direction configurations:

When the prescribed wind direction changes, the active sub-domain and its boundary assignments are updated accordingly. Fig. 4 (b) shows the configuration adopted after a forty-five-degree clockwise shift from a north wind to a northeast wind. The previously active north–south rectangle has been deactivated, and a new rectangle aligned with the northeast–southwest axis has been activated within the same envelope. The northeast-facing face of the new active region is assigned as the velocity inlet, and the southwest-facing face is assigned as the pressure outlet. Because the envelope was originally sized so that any direction-aligned rectangle fits entirely inside it, this reconfiguration involves no remeshing and no interpolation between grids. The mesh experienced by the new active region is the same mesh that was used for the previous direction; only the set of participating cells and the labeling of inlet and outlet faces have changed.

4. APPLICATION AND RESULTS

The framework was applied to a demonstration scenario in which the wind direction is initially aligned with the west-southwest (WSW) and then is shifted to the west-northwest (WNW) direction (a clockwise rotation of approximately thirty-four degrees) at a specified switching time during the release. The release magnitude, source elevation, and nuclide spectrum were held fixed across the analysis so that observed differences in the concentration output are attributable to the wind-direction transient and to its treatment in the CFD model. The simulations reported here focus on the wind-field response to the directional shift and on the resulting evolution of concentration fields at the EAB.

4.1. Reference Wind Field Before the Shift

Fig. 5 shows the velocity-vector field for the WSW-wind reference state once the simulation has reached a statistically quasi-stationary condition. Fig. 5 (a) presents a top-view of the full computational domain, confirming that the WSW inflow has been established across the entire active sub-domain. Fig. 5 (b) provides a close-up view of the plant-site vicinity, where the vector arrangement reflects the expected near-field response: incident flow from the west-southwest is deflected around the reactor buildings, recirculation cells form in the lee of the turbine buildings, and the wake of the building complex extends

downstream toward the east-northeast. This reference state is the starting point used to characterize the transient that follows.

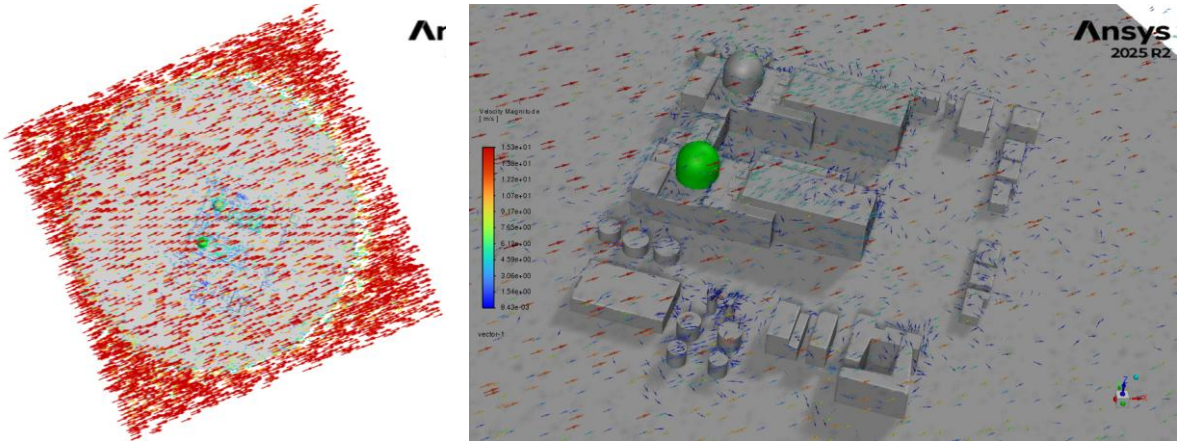

(a) Top view of the full computational domain showing the developed WSW inflow;

(b) Close-up view around the plant structures showing building-induced flow deflection, recirculation, and wake development.

Fig. 5. Quasi-stationary velocity-vector field for the north-wind reference state

4.2. Transient Wind-Field Response to the Direction Shift

Following the switch from the WSW to the WNW direction at the prescribed instant, the dispersion pattern of Lagrangian particles released from the source evolves over a finite adjustment interval rather than redirecting instantaneously. Fig. 6 collects six particle-track snapshots, colored by particle residence time, at t = 0, 20, 40, 60, 90, and 150 seconds relative to the moment of the wind-direction switch, in order to make the progression visible at multiple stages of the adjustment.

The snapshot sequence reveals three distinct phases in the transient particle response. In the first phase (t = 0 s to approximately 60 s), the carrier-phase momentum change associated with the new WNW inflow has not yet propagated to the region where the bulk of the particles reside. At t = 0 s (Fig. 6 (a)), the particle cloud is fully aligned with the prior WSW-to-ENE direction under quasi-stationary conditions. At t = 20 s (Fig. 6 (b)), although the boundary conditions have already been updated to reflect the new wind direction, the particle dispersion pattern remains essentially unchanged because the momentum of the prior wind state still dominates the local flow field in the vicinity of the particle cloud. At t = 40 s (Fig. 6 (c)) and t = 60 s (Fig. 6 (d)), the particle distribution in the core plume region continues to reflect the prior wind direction; however, a secondary effect becomes visible as the active computational sub-domain is reconfigured—the deactivation of the prior-direction sub-domain and the activation of the new-direction sub-domain introduce new boundary faces, and particles that reach these newly exposed boundaries begin to exit the domain, producing visible particle losses along edges that did not previously exist.

In the second phase (around t = 90 s, Fig. 6 (e)), the momentum associated with the WNW inflow has propagated sufficiently far into the domain to reach the region where the particles are concentrated. The primary transport direction of newly released particles shifts noticeably toward the ESE, and the particle dispersion footprint begins to reorient accordingly. In the third phase (t = 150 s, Fig. 6 (f)), the reorientation is essentially complete: the particle dispersion pattern is aligned with the new WNW-to-ESE direction, and the flow field has settled into a state consistent with the updated boundary conditions. The persistence of the prior-direction particle trajectories during the first phase, spanning roughly one to two minutes after the switch, is precisely the behavior that motivates the special boundary treatment described in Section 3.3.

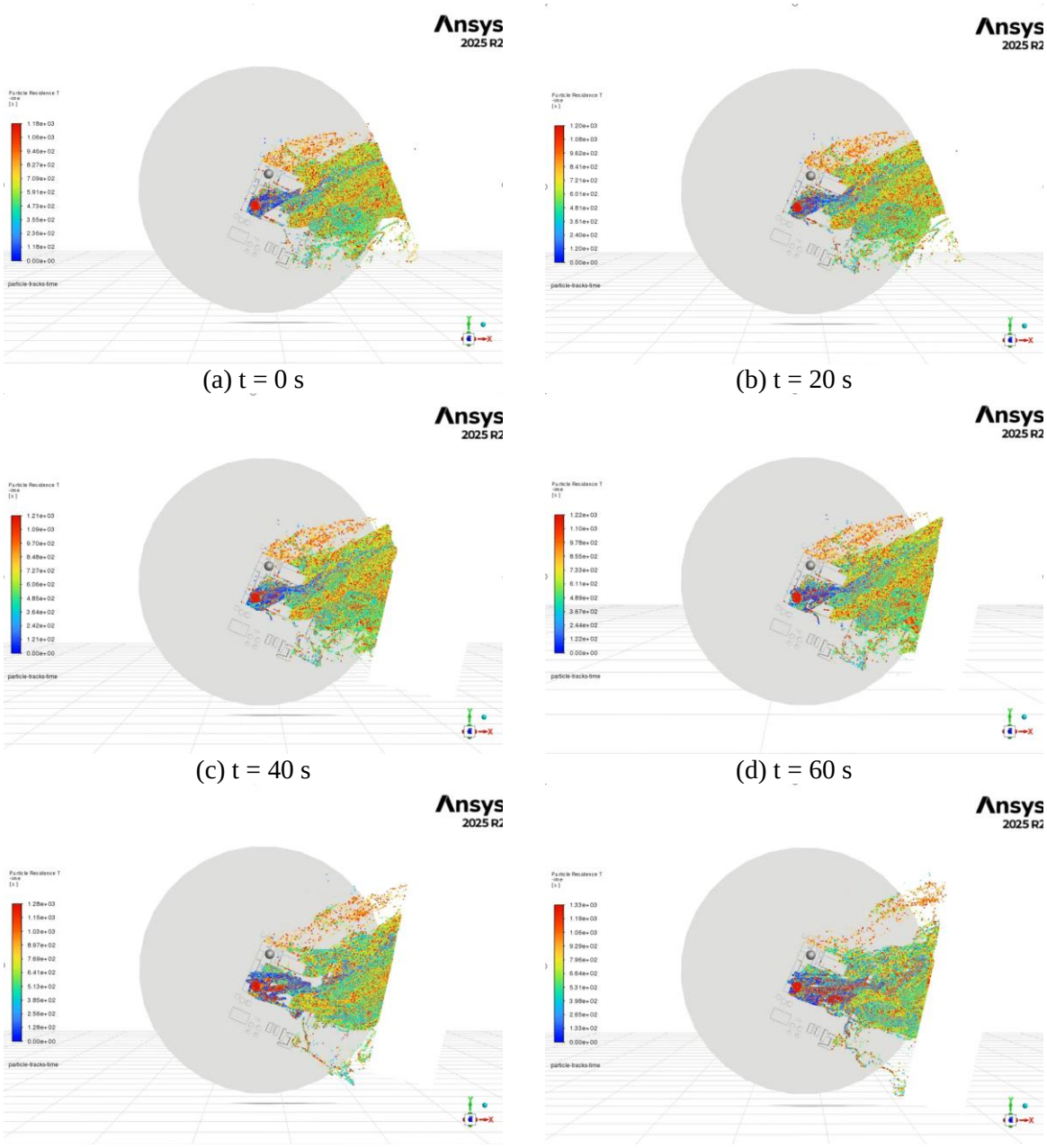

(a) t = 0 s (b) t = 20 s

(c) t = 40 s (d) t = 60 s

(e) t = 90 s (f) t = 150 s

Fig. 6. Particle-track snapshots colored by residence time at successive instants relative to the wind-direction switch from WSW to WNW: (a) immediately before the switch; (b)–(d) early transient phase in which the prior-direction momentum has not yet reached the main particle cloud; (e) onset of plume reorientation as the new wind-direction momentum arrives; (f) fully reoriented dispersion pattern aligned with the WNW inflow.

4.3. Implications for Concentration Variability

From the perspective of near-field particle dispersion behavior, the snapshot sequence in Fig. 6 has two practical consequences. The first concerns the timing of the concentration peak at any given EAB receptor. Because the wind-field transition is not instantaneous, the location of the dispersion centerline migrates continuously between sectors during the adjustment window rather than jumping from one sector to another. Receptors located in the angular range traversed by the migrating centerline therefore experience a concentration pulse of finite duration as the particle cloud sweeps across them, while receptors well outside that angular range experience essentially no contribution from the transient. The temporal peak concentration at a sector therefore depends not only on the initial and final wind

directions but also on how quickly the centerline traverses the intervening angular range, which in turn is set by the transition treatment.

The second consequence concerns the receptor-to-receptor spread of time-integrated concentration. If the wind direction had been assumed to change instantaneously from north to northeast, the receptors in the south sector (the original downwind direction) would receive most of their cumulative exposure during the pre-switch interval, and the receptors in the southwest sector (the new downwind direction) would receive most of theirs during the post-switch interval, with little overlap. The transient adjustment captured in the present framework smears this idealization: receptors in the intermediate sectors (south-southwest) accumulate appreciable exposure during the adjustment window, while receptors at the extremes accumulate slightly less than the instantaneous-switch idealization would predict. The receptor-to-receptor spread of time-integrated concentration is therefore lower under a realistic transient treatment than under an instantaneous-switch idealization, even though the temporal peak concentration at individual receptors may be higher because of the moving-cloud effect.

These observations have direct implications for protective-action decision making at the EAB. A consequence assessment built on a single-direction assumption will systematically underestimate the angular extent of the affected sector set and will overstate the contrast between maximally and minimally affected sectors. Both biases are conservative in the sense that protective actions selected on their basis are more restrictive than what the realistic transient field would warrant, but the magnitude of the conservatism is not uniform across sectors and depends on the timing of the wind shift relative to the release. The framework presented here is intended to make this dependence visible and quantifiable for site-specific assessments.

5. Summary and Conclusion

A CFD-based framework has been developed for evaluating radionuclide concentration variability at the Exclusion Area Boundary when the wind direction undergoes short-term transient changes during a release. The framework combines an envelope computational domain that admits arbitrary wind directions without remeshing, an active-domain reconfiguration scheme that maintains temporal continuity of the velocity field across direction switches, a pressure-outlet–based transition treatment that dissipates residual momentum without producing spurious reverse flow, and Lagrangian particle tracking that provides time-resolved concentration fields at sixteen sector-aligned receptors along the EAB.

Application to the Saeul Units 1 and 2 site under a representative WSW-to-WNW wind shift confirmed that the velocity field requires a finite adjustment window of approximately one to two minutes rather than reorienting instantaneously, that the dispersion centerline migrates continuously across intermediate EAB sectors during this window, and that the temporal peak concentration and the time-integrated concentration spread across receptors are both sensitive to the manner in which the wind-direction transient is represented. These findings indicate that an EAB concentration assessment built on a fixed-direction CFD analysis cannot be expected to capture the angular reach or the sector-to-sector contrast that a realistic transient wind sequence would produce.

Future work will extend the present analysis to scenarios in which multiple successive direction changes occur within a single release window, examine the sensitivity of the concentration metrics to the duration of the adjustment treatment, incorporate gaseous-phase radionuclide transport in addition to the aerosol-phase particle tracking presented here, implement surface deposition and resuspension mechanisms within the CFD framework to capture the full cycle of ground-level contamination and secondary airborne release, and ultimately perform dose conversion to connect the receptor-level concentration output to protective-action effectiveness models.

Acknowledgements

This research was supported by the grants of the Korea Institute of Radiological and Medical Sciences, funded by Nuclear Safety and Security Commission (No. 50090–2026), Republic of Korea.

This study was supported by the Nuclear Safety Research Program through the Regulatory Research Management Agency for SMRs(RMAS) and the Nuclear Safety and Security Commission(NSSC) of the Republic of Korea.(No. RS-2026-02310628)

References

[1] P. A. B. de Sampaio, M. A. G. Junior, and C. M. F. Lapa, "*A CFD approach to the atmospheric dispersion of radionuclides in the vicinity of NPPs*," Nuclear Engineering and Design, Vol. 238, pp. 250–273, (2007).
[2] S. He, Z. Zhao, S. Ni, W. Deng, and J. Zhao, "*A CFD study on radionuclides diffusion and dose assessment in Daya Bay nuclear power plant*," Progress in Nuclear Energy, Vol. 173, (2024).
[3] U.S. Nuclear Regulatory Commission, "*Atmospheric Relative Concentrations for Control Room Radiological Habitability Assessments at Nuclear Power Plants*," Regulatory Guide 1.194, (2003).
[4] K. F. Eckerman and J. C. Ryman, "*External Exposure to Radionuclides in Air, Water, and Soil*," Federal Guidance Report No. 12, EPA-402-R-93-081, (1993).
[5] G. Kim and S.Y. Kim, "*Comparative Analysis of Near-Field Atmospheric Dispersion Models for Nuclear Emergency Planning Zone Sizing*," Transactions of the Korean Nuclear Society Spring Meeting, Jeju, Korea, May 7–8, (2026).